Hindawi Publishing Corporation
EURASIP Journal on Advances in Signal Processing
Volume 2008, Article ID 747325, 13 pages
doi:10.1155/2008/747325

Research Article

Cancelling ECG Artifacts in EEG Using a Modified Independent Component Analysis Approach

Stéphanie Devuyst,[1] Thierry Dutoit,[1] Patricia Stenuit,[2] Myriam Kerkhofs,[2] and Etienne Stanus[3]

[1] *TCTS Lab, Faculté Polytechnique de Mons, 31 Boulevard Dolez, 7000 Mons, Belgium*
[2] *Sleep Laboratory, CHU de Charleroi, Vésale Hospital, Université Libre de Bruxelles, Rue de Gozée 706, 6110 Montigny-le-Tilleul, Belgium*
[3] *Computer Engineering Department, CHU Tivoli Hospital, 7100 La Louvière, Belgium*

Correspondence should be addressed to Stéphanie Devuyst, stephanie.devuyst@fpms.ac.be

Received 3 April 2008; Revised 11 July 2008; Accepted 31 July 2008

Recommended by Kenneth Barner

We introduce a new automatic method to eliminate electrocardiogram (ECG) noise in an electroencephalogram (EEG) or electrooculogram (EOG). It is based on a modification of the independent component analysis (ICA) algorithm which gives promising results while using only a single-channel electroencephalogram (or electrooculogram) and the ECG. To check the effectiveness of our approach, we compared it with other methods, that is, ensemble average subtraction (EAS) and adaptive filtering (AF). Tests were carried out on simulated data obtained by addition of a filtered ECG on a visually clean original EEG and on real data made up of 10 excerpts of polysomnographic (PSG) sleep recordings containing ECG artifacts and other typical artifacts (e.g., movement, sweat, respiration, etc.). We found that our modified ICA algorithm had the most promising performance on simulated data since it presented the minimal root mean-squared error. Furthermore, using real data, we noted that this algorithm was the most robust to various waveforms of cardiac interference and to the presence of other artifacts, with a correction rate of 91.0%, against 83.5% for EAS and 83.1% for AF.

1. INTRODUCTION

Electrocardiogram (ECG) artifacts occur when the relatively high cardiac electrical field affects the surface potentials on the scalp and near the eyes. This leads to interference on the electroencephalograms (EEG) and electrooculograms (EOG) which can easily be recognized by its periodicity and its coincidence with the ECG peaks (Figure 1). Its waveform can vary from derivation to derivation, and large interindividual voltage variations can be observed [1].

ECG artifacts over EEG signals constitute a serious problem for the automatic interpretation and analysis of polysomnographic signals. Hence, some methods have been developed for removing them. Fortgens and De Bruin [2] proposed an algorithm whereby the correction was made by subtracting a linear combination of four ECG derivations. The weights of this combination were calculated so as to minimize the EEG variance after subtraction. This method was also tested by Lanquart et al. [3] although they used only one ECG derivation.

The ensemble average subtraction (EAS) method was described and used by Nakamura and Shibasaki [4], Harke et al. [5], and Park et al. [6]. In this approach, an average ECG-artifact waveform was computed for each homogeneous EEG portion, and an estimate of the artifact was generated by repeating this template synchronously with the interference peaks. This signal was then subtracted from the contaminated EEG to correct it.

Sahul et al. [7] introduced artifact cancellation by adaptive filtering (AF) using an ECG channel reference. Strobach et al. [8] showed that this method was not appropriate if the ECG and the real interference exhibit remarkably different waveforms. They introduced a two-pass adaptive filtering algorithm, where an artificial reference was first generated by ensemble averaging to be more related to the real interference than the ECG. This idea was taken up by Cho et al. [9] who also used a least square acceleration filter to better detect the *R*-peaks positions before generating the artificial signal of *R*-peak synchronized pulse.

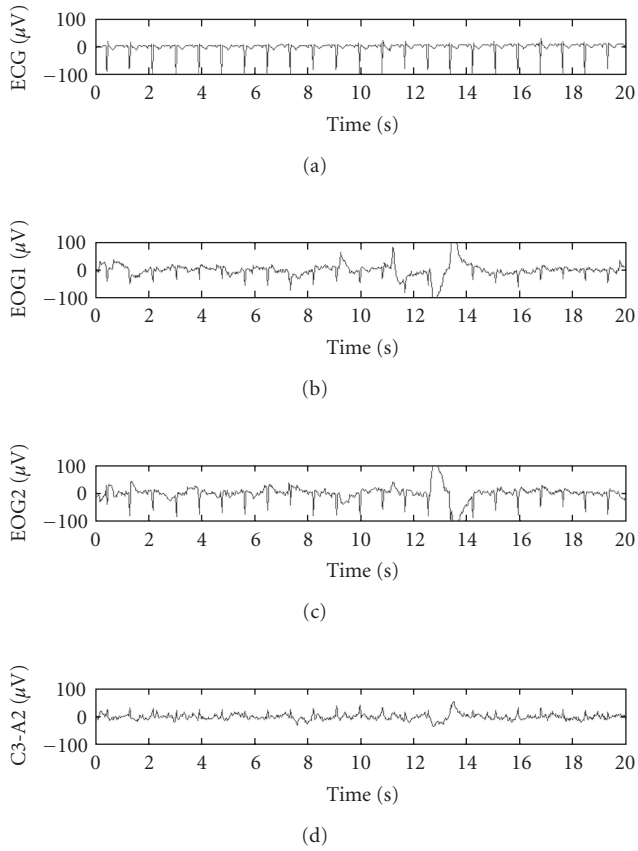

Figure 1: ECG artifact on EOG1, EOG2, and C3-A2.

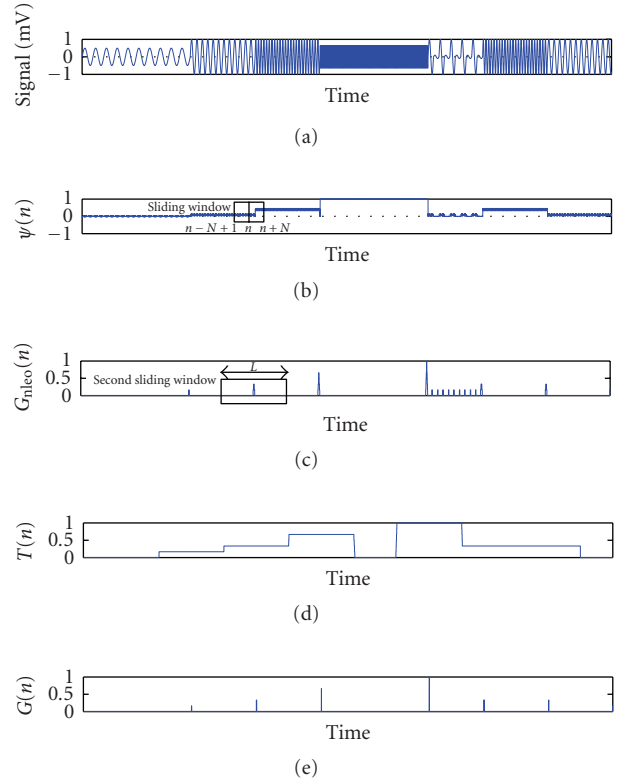

Figure 2: Generation of a trigger from the ECG: illustration on an artificial signal composed of sinusoids with variable amplitudes and frequencies (see main text for details on the signals shown).

Morphological filters (MFs) were tested for the removal of ECG artifacts by Lanquart et al. [3]. The idea is to define an artifact template called "structuring element" and to probe the contaminated EEG to quantify how the structuring element fits within the signal. This enables to detect the artifact parts of the signal to remove. Unfortunately, MFs are known to also eliminate other actual waves that are not ECG artifacts. Their use, thus, requires a second phase of correction to distinguish the actual waves from the interferences and to restore them to the corrected EEG signal.

Finally, some authors investigated the use of independent component analysis (ICA) to cancel ECG noise [3, 10–13]. However, either their methods required many EEG channels and implied to visually select the origin of cardiac interference among estimated sources, or their methods were found to be somehow inefficient since the artifact was reduced but still visible.

In this paper, we introduce a new algorithm resulting from a modification of the ICA method. The algorithm gives promising results while using only a single-channel EEG (or EOG) and the ECG. To check its effectiveness, we have also implemented the EAS and AF methods and compared their correction rate, their computational load, and their robustness to the new algorithm.

Section 2 describes these ECG artifact correction algorithms in detail. Section 3 presents experimental results. Section 4 discusses these results and concludes this paper.

2. METHODS

2.1. Ensemble average subtraction (EAS)

The first step of the ensemble average subtraction (EAS) algorithm consists in generating a trigger from the ECG by QRS detection. The method we are used is partly based on [14], which used a nonlinear energy operator to achieve a segmentation of the EEG into quasistationary fragments. This is illustrated in Figures 2 and 3.

A nonlinear energy operator is first applied to the ECG signal $s(n)$ as follows:

$$\psi[n] = s(n-1)*s(n-2) - s(n)*s(n-3). \quad (1)$$

The corresponding output, called *frequency-weighted energy* ψ, is proportional to the frequency and the amplitude of the signal s. By using a sliding time-domain window where the frequency-weighted energy in the left part is subtracted from that of the right part at each time instant n, it is possible to obtain a function $G_{\text{nleo}}(n)$ which emphasizes the ECG R-waves:

$$G_{\text{nleo}}(n) = \left| \sum_{m=n-N+1}^{n} \psi(m) - \sum_{m=n+1}^{n+N} \psi(m) \right|, \quad (2)$$

where the total window size is $2N$ samples.

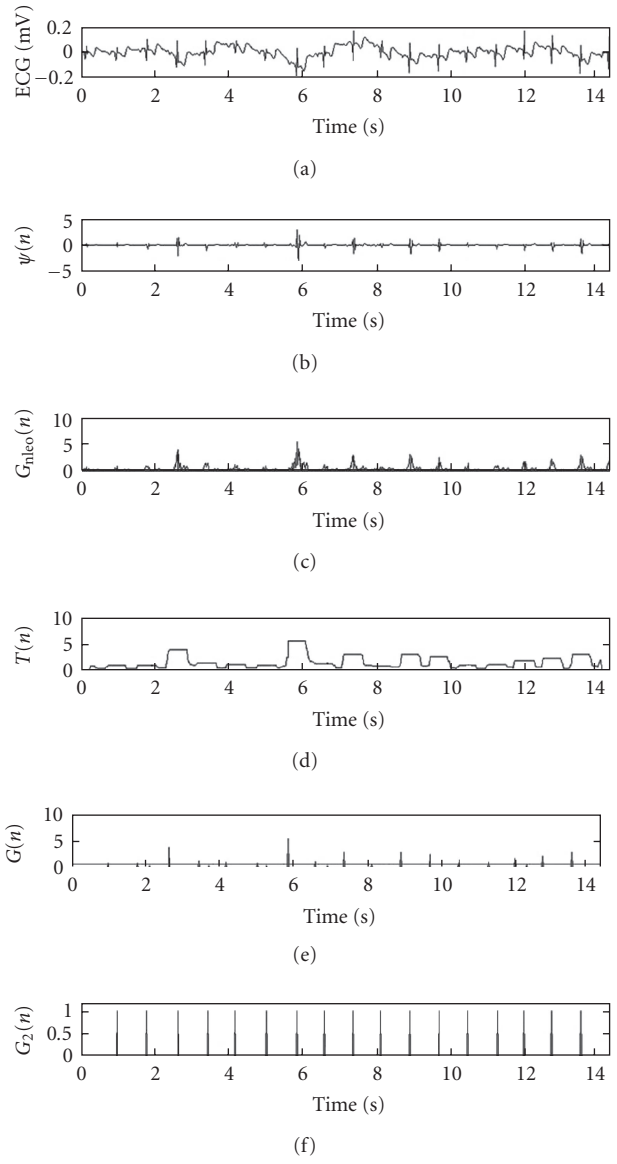

Figure 3: Generation of a trigger from the ECG: application to a real ECG channel (see main text for details on the signals shown).

A second sliding window is used on $G_{\text{nleo}}(n)$ and each sample $G_{\text{nleo}}(n)$ is replaced by the maximum value of $G_{\text{nleo}}(n)$ in the window:

$$T(n) = \begin{cases} \max\left[G_{\text{nleo}}\left(n-\frac{L}{2} : n+\frac{L}{2}\right)\right] & \text{for } n=\frac{L}{2}, \left(\frac{L}{2}+1\right), \dots \\ 0 & \text{for } n=0,1,\dots\left(\frac{L}{2}-1\right). \end{cases} \quad (3)$$

The resulting signal $T(n)$ is then compared to $G_{\text{nleo}}(n)$ to obtain a trigger function:

$$G(n) = \begin{cases} G_{\text{nleo}}(n), & \text{if } G_{\text{nleo}}(n) \geq T(n), \\ 0, & \text{if } G_{\text{nleo}}(n) < T(n). \end{cases} \quad (4)$$

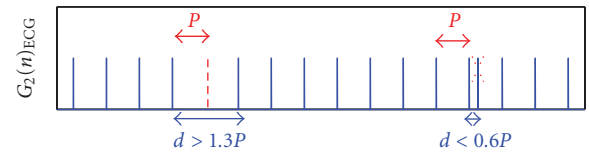

Figure 4: Removal of the erroneous peaks and addition of the missing positions.

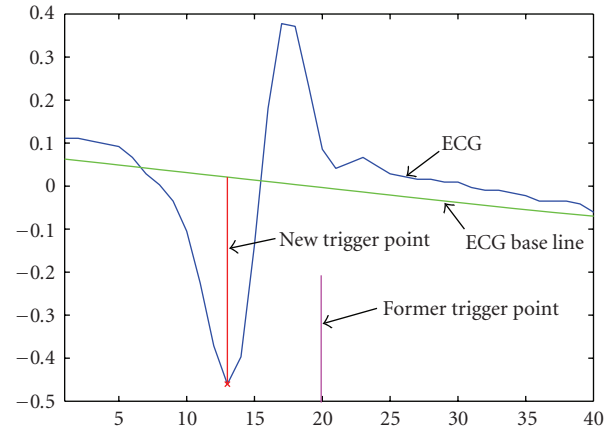

Figure 5: Adjustment of the position of the R-peak: the new trigger point is set to the place, where the difference between the ECG and its base line is maximum.

Finally, the number of false detections is reduced by applying a threshold to $G(n)$, derived from the average of its peaks:

$$G_2(n) = \begin{cases} G(n), & \text{if } G(n) \geq \text{mean } (G(n) \neq 0), \\ 0, & \text{if } G(n) < \text{mean } (G(n) \neq 0). \end{cases} \quad (5)$$

To improve this detection process inspired by [14], we also use the periodic characteristic of the cardiac beat: when two peaks in $G_2(n)$ are separated by less than 0.6 times the average cardiac period P, the most likely peak position is considered to be the closest to the point delayed by one period from the preceding spike; and if no R-peak is found before 1.3^*P seconds from the preceding peak, a new trigger position is added after P seconds to fill the gap (Figure 4).

In practice, these new positions do not always correspond to the precise locations of R-peaks in the electrocardiogram. The surrounding of each presumed trigger point is, therefore, examined, and the correct position of the R-peak in this surrounding is set to the place where the difference between the ECG and its base line is maximum (Figure 5). The width of the examined surrounding must be sufficient to contain the real position of the R-peak, but not too large so as to avoid neighboring ECG waves. We set its width to 0.15 times the duration of the cardiac period.

We then obtain a trigger $G_2(n)$ indicating the positions of the R-peaks of the ECG. We will call it "ECG trigger" in the following.

The second step of the ensemble average subtraction algorithm is the generation of an estimate of the ECG artifact. For this purpose, the EEG (or EOG) signal is segmented

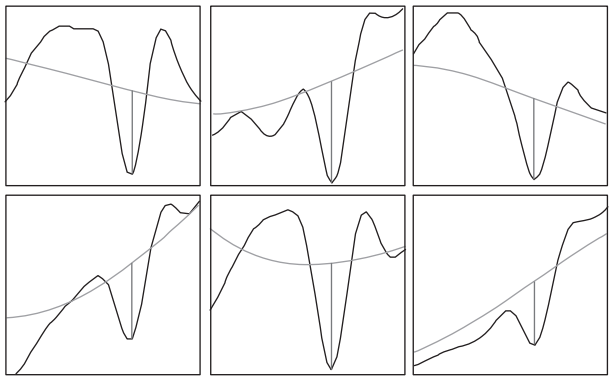

Figure 6: Positioning of an interference peak from an ECG triggering point: some examples.

into 20-second fragments. Assuming that subsequent heart beats produce sufficiently similar interference waveforms on each 20-second fragment and that EEG has zero-mean distribution, one can compute an estimate of the ECG artifact waveform by averaging segments of corrupted signal located around each interference peak in the 20-second fragment. The duration of the averaging fragments (20 seconds) was chosen as a compromise; it is long enough to separate the artifact from the underlying EEG and short enough to ensure similar interference waveforms. The duration of the segments located around each interference peak was fixed to 0.85 times the duration of the mean cardiac period estimated on the 20-second fragments of the ECG trigger.

The exact location of interference peaks on the EEG signal is calculated from the ECG trigger. Like previously, the bias error between the exact position of the interference and the ECG triggering point is corrected by examining the EEG signal surrounding the trigger point. The location of the interference is set so as to maximize the difference between the EEG and its base line. Some examples are illustrated on Figure 6. Notice the importance of using a sufficiently narrow surrounding, in order for the final interference location not to be influenced by the EEG background (which can exhibit important variations).

The last step of the method consists in subtracting this ensemble average from each interference peak of the contaminated EEG. In practice, it is better to multiply the ensemble average by a Hanning window before subtraction to avoid introducing discontinuities.

2.2. Adaptive filtering (AF)

The classical structure of an adaptive filter used to correct the ECG artifact from an EEG signal is illustrated on Figure 7. A reference signal $x(n)$ (i.e., the ECG channel) is passed through an adaptive FIR filter $A_p(z)$ to obtain an optimal approximation of the cardiac interference $b(n)$:

$$A_p(z) = a_0 + a_1 z^{-1} + a_2 z^{-2} + \cdots + a_p z^{-p}. \quad (6)$$

This approximation is subsequently subtracted from the corrupted signal to produce an estimate of the true EEG.

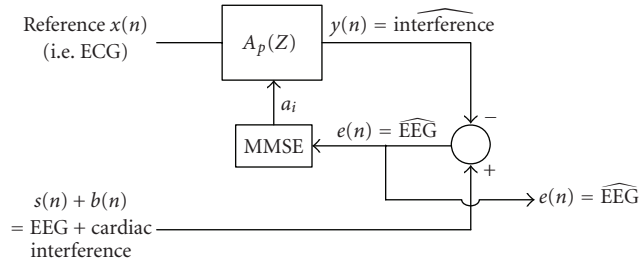

Figure 7: ECG artifact correction by adaptive filtering.

Under the assumptions that the original EEG signal $s(n)$ is not correlated with the cardiac interference $b(n)$ and that the average of the interference $E[b(n)]$ is equal to the average of its estimate $E[y(n)]$, the minimization of the average of the quadratic error (minimum mean squared error (MMSE)) can be used for the adaptation of the filter weights [15, 16].

The underlying assumption is that the interference can be well approximated by applying a simple FIR to the reference signal $x(n)$. This is not always the case when the ECG is directly used as the reference signal. Indeed, the interference and ECG signals can sometimes exhibit remarkably different waveforms (to different to be approximated by an FIR filter), although they are synchronized temporally.

Strobach et al. [8], therefore, suggested using an artificial reference signal generated by convoling the average artifact waveform with the ECG trigger:

$$x(n) = a(n) * G_2(n), \quad (7)$$

where $x(n)$ is the artificial reference signal (see an example in Figure 8(c)), $G_2(n)$ is the ECG trigger computed as in the EAS method, and $a(n)$ is the average artifact waveform recomputed for each 20-second fragment, by averaging segments of corrupted signal located around each interference peak.

In this work, we tested these two approaches.

2.3. Independent component analysis (ICA)

Independent component analysis (ICA) was developed some years ago in the context of blind source separation. Its aim is to estimate N source signals $s_1(t), s_2(t), \ldots, s_N(t)$ unknown but assumed to be statistically independent from the observation of M signals $x_1(t), x_2(t), \ldots, x_M(t)$ which result from a mixture of the underlying sources signals.

ICA requires at least as many mixtures as there are independent sources ($M \geq N$). In our case, we suppose M equals to N, and we try to estimate the original EEG and the original interference (the two source signals) from two observed signals: the ECG and the corrupted EEG.

In the simplest case, the mixture is supposed to be linear and instantaneous, so that observations at time instant t result from a linear combination of the sources at that instant:

$$x_i(t) = \sum_{j=1}^{N} a_{ij} s_j(t) \quad i = 1 \cdots M. \quad (8)$$

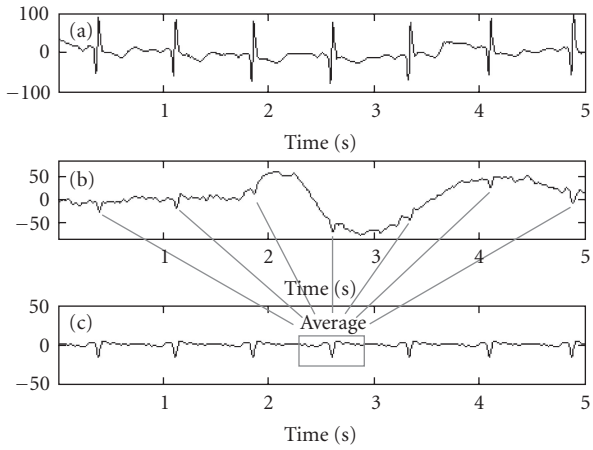

Figure 8: (a) ECG, (b) EEG corrupted by ECG artifact, (c) artificial reference used for AF.

This is clearly not the case here, as the interference peaks are not exactly synchronized with the R-peaks of the ECG. As a matter of fact, we found experimentally that applying ICA with such hypotheses on our observed signals did not lead to efficient correction of the cardiac artifacts. We, therefore, applied the so-called convolutive linear model, where the observations result from a linear mixture of the sources filtered by FIR filters:

$$\begin{aligned} x_i(t) &= \sum_{j=1}^{N} a_{ij}(t) * s_j(t) \quad i = 1 \cdots M \quad \xrightarrow{\text{discrete case}} \\ x_i(n) &= \sum_{j=1}^{N} \sum_{k=0}^{K} a_{ij}(k)\, s_j(n-k) \quad i = 1 \cdots M, \end{aligned} \tag{9}$$

where $a_{ij}(t)$ (or $a_{ij}(k)$ in the discrete case) is the transfer function between the jth source and the ith sensor and K is the highest order of the FIR filters.

As illustrated on Figure 9, the purpose of ICA in this case is to find a source separation system, whose outputs should be equal to the original sources:

$$\begin{aligned} s_j(t) \approx y_i(t) &= \sum_{j=1}^{N} w_{ij}(t) * x_j(t) \quad \xrightarrow{\text{discrete case}} \\ s_j(n) \approx y_i(n) &= \sum_{j=1}^{N} \sum_{k=0}^{K} w_{ij}(k)\, x_j(n-k). \end{aligned} \tag{10}$$

By using the FIR linear algebra notation, (9) and (10) can be written as

$$\begin{aligned} \mathbf{x_t} &= \mathbf{A}\, \mathbf{s_t}, \\ \mathbf{s_t} \approx \mathbf{y_t} &= \mathbf{W}\, \mathbf{x_t}, \end{aligned} \tag{11}$$

where the element $A_{ij}(z)$ of the mixing matrix $\mathbf{A}$ corresponds to the transfer function between the jth source and the ith sensor, and the element $W_{ij}(z)$ of the separating matrix $\mathbf{W}$ corresponds to the transfer function between the jth sensor and the ith estimated source. In the FIR linear algebra notation, matrices are composed of FIR filters instead of scalars, and the multiplication between two FIR matrix elements is defined as their convolution.

For example, by using the FIR linear algebra notation, equation $\mathbf{x_t} = \mathbf{A}\, \mathbf{s_t}$ expresses

$$\begin{aligned} \begin{bmatrix} x_1(n) \\ \vdots \\ x_M(n) \end{bmatrix} &= \begin{bmatrix} a_{11}(t) & \cdots & a_{1N}(t) \\ \vdots & \ddots & \vdots \\ a_{MN}(t) & \cdots & a_{MN}(t) \end{bmatrix} \cdot \begin{bmatrix} s_1(t) \\ \vdots \\ s_N(t) \end{bmatrix} \\ &= \begin{bmatrix} \sum_{j=1}^{N} a_{1j}(t) * s_j(t) \\ \vdots \\ \sum_{j=1}^{N} a_{Mj}(t) * s_j(t) \end{bmatrix} \xrightarrow{\text{discrete case}} \\ \begin{bmatrix} x_1(n) \\ \vdots \\ x_M(n) \end{bmatrix} &= \begin{bmatrix} \sum_{j=1}^{N} \sum_{k=0}^{K} a_{1j}(k) s_j(n-k) \\ \vdots \\ \sum_{j=1}^{N} \sum_{k=0}^{K} a_{Mj}(k) s_j(n-k) \end{bmatrix}. \end{aligned} \tag{12}$$

To find the unknown separating matrix $\mathbf{W}$, Bell and Sejnowski [17] proposed to maximize the joint entropy $H(\mathbf{g})$ of the vector $\mathbf{g_t} = [g_1(t), g_2(t), \ldots, g_N(t)]^T$, whose components $g_i(t) = g(y_i(t)) \approx F_s(y_i(t))$ are the sources $y_i(t)$ transformed by a sigmoid function g which approximates to the cumulative density function F_s of the sources (seen as random signals). In the convolutive case, this suggests to work with a feedforward architecture, as illustrated on Figure 10.

A common choice for the sigmoid function g is the logistic function $g(y_i) = (1 + \exp(-y_i))^{-1}$ or the hyperbolic tangent function $g(y_i) = \tanh(y_i)$. In this work, we tested these two possibilities.

The separating matrix which maximizes the joint entropy $H(\mathbf{g})$ can be found by a gradient ascent algorithm which consists, in the discrete case, in iterating on:

$$\begin{aligned} w_{ij}(k) &\longleftarrow w_{ij}(k) + \mu \frac{\partial H(\mathbf{g})}{\partial w_{ij}(k)} \\ &\forall i, j \in [1, \ldots, N] \;\; \forall k \in [0, \ldots, K], \end{aligned} \tag{13}$$

where μ is the learning rate and $w_{ij}(k)$ is the kth coefficient of the impulse response of the FIR filter between the jth sensor and the ith-estimated source; K is the highest order of the FIR filters.

Torkkola [18] has shown that this results in iterating on:

$$\begin{aligned} w_{ij}(k) &\longleftarrow w_{ij}(k) \\ &+ \mu \begin{cases} E\left[\dfrac{1}{\det(\mathbf{W}_{k=0})} \cdot (-1)^{i+j} \cdot \Delta_{ij}(0) + \dfrac{\partial p_s(y_i)}{\partial F_s(y_i)} \cdot x_j \right] \\ \qquad\qquad \text{for } k = 0, \\ E\left[\dfrac{\partial p_s(y_i)}{\partial F_s(y_i)} \cdot x_{j_{[-k]}} \right] \quad \text{for } k \neq 0 \;\; \forall i, j \in [1, \ldots, N] \end{cases} \end{aligned} \tag{14}$$

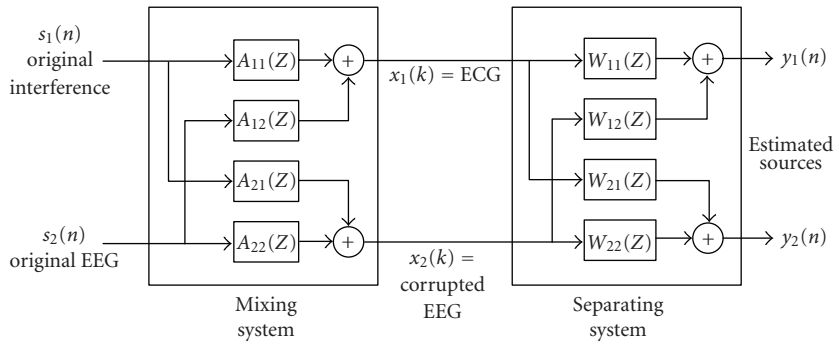

Figure 9: Convolutive linear mixture of two sources and the corresponding source separation system.

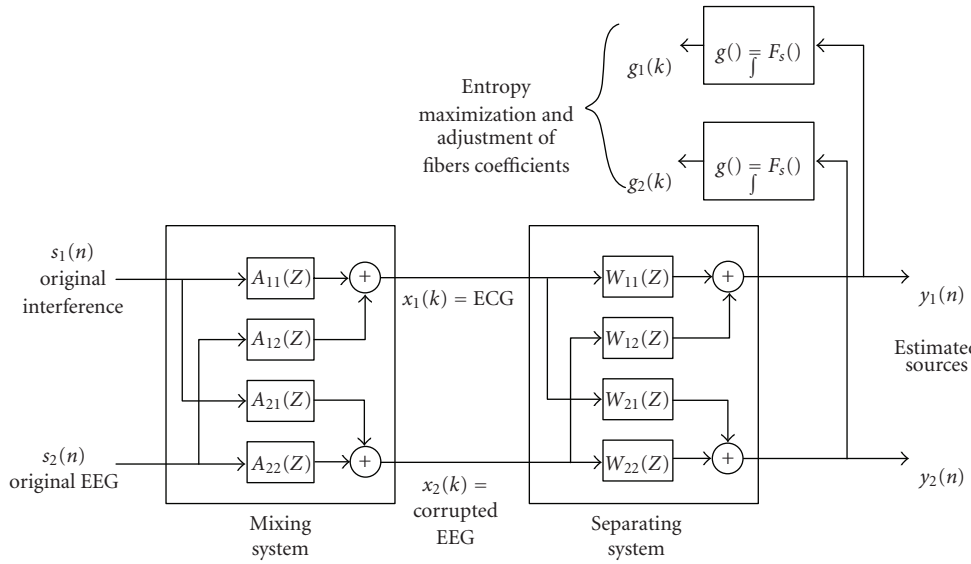

Figure 10: Network architecture for ICA based on the maximization of the joint entropy.

with

$$\mathbf{W}_{k=0} = \begin{bmatrix} w_{11}(0) & \cdots & w_{1N}(0) \\ \vdots & \ddots & \vdots \\ w_{N1}(0) & \cdots & w_{NN}(0) \end{bmatrix}, \tag{15}$$

where $\det(\mathbf{W}_{k=0})$ is the determinant of the matrix $\mathbf{W}_{k=0}$, $\Delta_{ij}(0)$ is the determinant of the matrix obtained by removing the ith row and the jth column from $\mathbf{W}_{k=0}$, $F_s(y_i) = g(y_i)$, $p_s(y_i) = \partial g(y_i)/\partial y_i$, and $E[\cdot]$ is the mathematical expectation.

For the logistic function, we have $p_s(y_i)=g(y_i)\cdot(1-g(y_i))$ and $\partial p_s(y_i)/\partial F_s(y_i) = 1 - 2g(y_i)$, and for the hyperbolic tangent function, we have $p_s(y_i) = 1 - g^2(y_i)$ and $\partial p_s(y_i)/\partial F_s(y_i) = -2g(y_i)$.

We implemented this algorithm and noted experimentally that it has some difficulties to converge toward the correct solution, especially when the sampling rate is high. We, therefore, considered an additional hypothesis to improve the convergence; we supposed that the interference which on the EEG is a filtered version of the first observed signal (the ECG). The resulting architecture is illustrated on Figure 11, with a mixing matrix of the form:

$$\mathbf{A} = \begin{pmatrix} h_{\text{impulse}} & 0 \\ h & h_{\text{impulse}} \end{pmatrix}, \tag{16}$$

and a separating matrix of the form:

$$\mathbf{W} = \begin{pmatrix} h_{\text{impulse}} & 0 \\ -h & h_{\text{impulse}} \end{pmatrix}, \tag{17}$$

where $h_{\text{impulse}} = \{1\ 0\ 0\ 0\ 0\ 0 \cdots\}$ is the identity filter and h corresponds to the unknown interference shaping.

The iterative algorithm simplifies to:

$$w_{21}(k) \longleftarrow w_{21}(k) + \mu \begin{cases} E\left[\dfrac{1}{\det(\mathbf{W}_{k=0})}\cdot(-1)\cdot\Delta_{21}(0) + \dfrac{\partial p_s(y_2)}{\partial F_s(y_2)}\cdot x_1\right] & \text{for } k = 0, \\ E\left[\dfrac{\partial p_s(y_2)}{\partial F_s(y_2)}\cdot x_{1_{[-k]}}\right] & \text{for } k \neq 0, \end{cases} \tag{18}$$

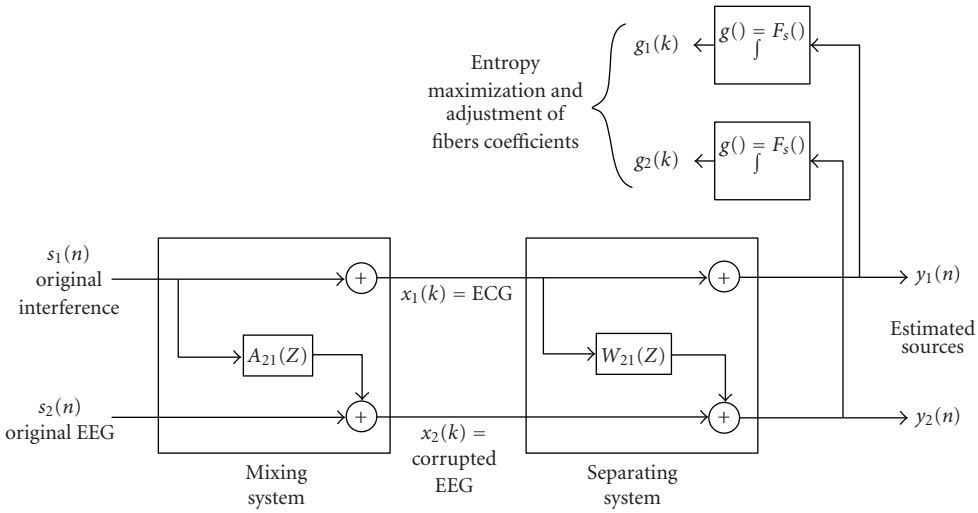

Figure 11: Network architecture for our modified ICA algorithm.

with

$$\mathbf{W}_{\text{initial}} = \begin{pmatrix} h_{\text{impulse}} & 0 \\ h_{\text{impulse}} & h_{\text{impulse}} \end{pmatrix}. \tag{19}$$

It should be noted that, while the additional assumption we make here is identical to the one made in the adaptive filtering approach, the separation criterion is completely different. This is why the results of these two methods will be different (as we will see in Section 3). It remains that this assumption can (like previously) be discussed if the interference waveform is remarkably different from that of the ECG. Thus, as in Section 2.2, we also tested the use of an artificial observed signal generated by repeating the average artifact waveform each time the ECG trigger is different from zero.

Notice that in this ICA-based approach, filter coefficients are supposed to be constant with time. Thus, we segmented the EEG signal into fragments in which the interference was supposed to be stationary. In each such fragment, we iterated on the values of the coefficients of h until convergence was reached to obtain optimal solution. However, in order to speed up the computations, we initialized each new $\mathbf{W}$ matrix with the coefficients obtained for the preceding fragment.

The fragments duration was set to 20 seconds; short enough to ensure the stationarity of the interference, and long enough to constrain the computational load and to not be influenced by other short artifacts.

3. RESULTS

3.1. Evaluation of the *R*-peak detector algorithm

Initially, we used the standard 24 hour-MIT/BIH arrhythmia database [19] to evaluate the new *R*-peak detector algorithm presented in the EAS methods. This database consists of 48 half-hour excerpts of two ECG recordings digitized at 360 Hz (here, we used only the first ECG channel). The recordings contain (among others) several less common but clinically significant arrhythmias. They were annotated by different cardiologists, and a common reference annotation was included in the database. Thus, more than 110 000 beat annotations were available to evaluate our algorithm. Since the reference annotation does not always point the exact position of the *R*-peak (but rather the position of the beat, see Figure 12(a)), we authorized a maximum difference of 0.1 second between the automatic *R*-peak detection and the reference annotation, during the sensitivity evaluation. Table 1 summarizes the performance of our *R*-peak detector algorithm on this database. The approach seems well founded since it reaches a global sensitivity of 97.95 percent. Nevertheless, less satisfactory results are obtained for recordings 208 and 221. This is due to the numerous premature ventricular contractions contained in these recordings and characterized by premature *R*-peaks of slighter slope (see an example on Figure 12(a), second 636). Indeed, their frequency-weighted energy is significantly smaller than the other normal *R*-peaks (Figure 12(b)), so that it is ignored during the further thresholding stage (Figure 12(c)). The resulting gap is filled by adding a new trigger position after P seconds, but this new position is too far from the real premature *R*-peak to be properly corrected. On Figure 12(a), we can see the bad automatically detected *R*-peak position around second 636 (indicated as "x"), compared to the reference annotation indicated by "o."

3.2. Comparison of the ECG artifact correction algorithms

In order to evaluate the performance of the proposed method, five algorithms were finally implemented and tested as follows:

(i) the ensemble average subtraction (EAS);

(ii) the adaptive filtering (AF-ECG), using an ECG reference;

Table 1: Results of evaluting the ECG *R*-peaks detection algorithm using the MIT/BIH database.

Tape (no.)	Total number of beats	Number of *R*-peaks not correctly detected	Sensitivity
100	2263	1	99.96
101	1859	3	99.84
102	2179	0	100.00
103	2077	5	99.76
104	2221	6	99.73
105	2564	15	99.41
106	2020	167	91.73
107	2130	19	99.11
108	1756	24	98.63
109	2523	5	99.80
111	2116	0	100.00
112	2530	0	100.00
113	1788	6	99.66
114	1870	7	99.63
115	1944	2	99.90
116	2403	9	99.63
117	1529	0	100.00
118	2270	0	100.00
119	1980	15	99.24
121	1855	3	99.84
122	2467	0	100.00
123	1512	3	99.80
124	1612	9	99.44
200	2593	35	98.65
201	1958	124	93.67
202	2127	61	97.13
203	2973	248	91.66
205	2647	19	99.28
207	1848	37	98.00
208	2945	318	89.20
209	2996	10	99.67
210	2640	102	96.14
212	2739	1	99.96
213	3240	6	99.81
214	2253	118	94.76
215	3352	11	99.67
217	2201	7	99.68
219	2146	14	99.35
220	2040	26	98.73
221	2419	354	85.37
222	2474	52	97.90
223	2596	220	91.53
228	2046	131	93.60
230	2247	0	100.00
231	1564	5	99.68
232	1774	7	99.61
233	3068	31	98.99
234	2744	3	99.89
48 patients	109098	2239	97.95

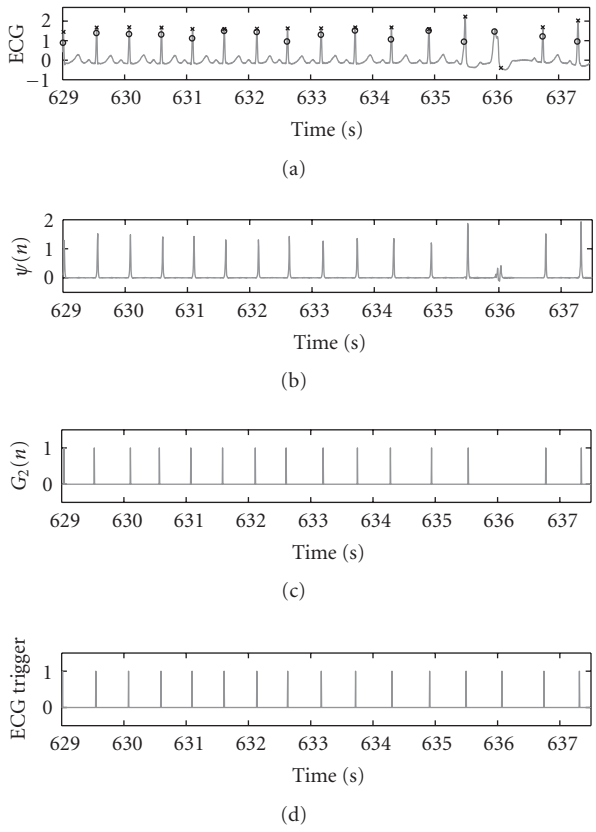

Figure 12: Generation of the ECG trigger on recording $n°208$ of the MIT/BIH database: (a) ECG with the reference annotation indicated by "o" and the automatic detection indicated by "x", (b) and (c) intermediate stages of the R-peak detection procedure (see main text for details on these signals) and (d) ECG trigger.

(iii) the adaptive filtering (AF-EA), using an artificial reference generated by ensemble averaging;

(iv) the independent component analysis (ICA-ECG), using the corrupted EEG and the ECG as observed signals;

(v) the independent component analysis (ICA-EA), using the corrupted EEG and an artificial signal generated by ensemble averaging as observed signals.

Tests were carried out on two different databases: a simulated one and a real one.

Simulated data

The simulated data were obtained by addition of a filtered ECG on a visually clean original EEG to create an artificial cardiac interference. The ECG and EEG extracts were acquired simultaneously from a healthy subject during 5 minutes. Sampling rate was 200 Hz. The filter used was of order 5 and the coefficients of its impulse response were randomly generated at each creation of an artificial signal. 60 extracts were created and their corresponding signal-to-noise ratios (SNRs) were computed. Next, each algorithm was applied to the simulated data, and the root mean squared error (RMSE) was computed between the cleaned EEG and the original artifact-free EEG.

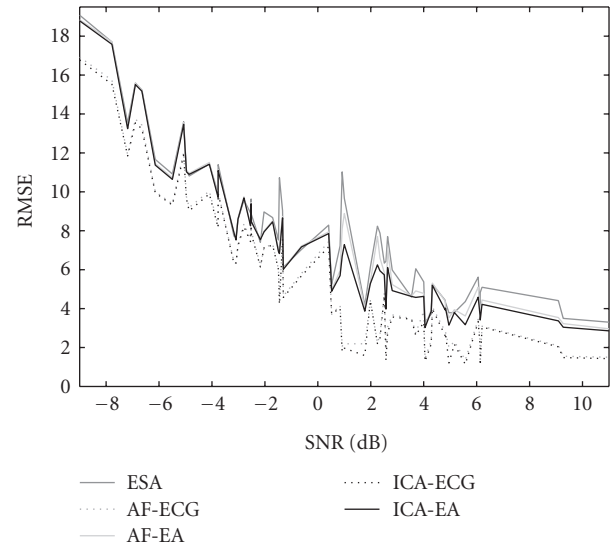

Figure 13: RSME according to SNR using simulated data with artificial ECG artifact.

Figure 13 shows the RMSE for each algorithm according to the SNR. We see that AF-ECG and ICA-ECG algorithms (in dotted lines) have the best performance. The reason is that simulated data (given their creation method) rigorously respect the assumption of these methods, that is, the interference can be well approximated by applying a simple FIR to the reference signal. Let us recall that this is not always the case with real data, where the interference can sometimes exhibit remarkably different waveforms from that of the ECG signals.

The other processes (EAS, AF-EA, and ICA-EA) give generally similar results. However, when differences can be observed between their RMSE, we notice that our new method (ICA-EA) always shows the best performance.

It is also visible in Figure 13 that, for each method, RMSE decreases according to the SNR. For an infinite SNR (i.e., by applying the process to the original artifact-free EEG), we have obtained relatively similar results ($\text{RMSE}_{\text{AF\_ECG}} = 1.6548$; $\text{RMSE}_{\text{AF\_EA}} = 1.3473$; $\text{RMSE}_{\text{ICA\_ECG}} = 1.2474$; $\text{RMSE}_{\text{ICA\_EA}} = 1.2509$) except for the EAS algorithm which presented a slightly higher RMSE ($\text{RMSE}_{\text{ESA}} = 2.6145$). These values are low but nonzero, that means that all methods introduce additional distortions even if they are not really detectable visually. It is thus not recommended to automatically use them, but to detect beforehand if a cardiac interference is present or not.

Real data

Real data used in this study were recorded at the Sleep Laboratory of the André Vésale hospital (Montigny-le-Tilleul, Belgium). They are composed of 10 excerpts of 15 minutes-long polysomnographic (PSG) sleep recordings, randomly selected during the night. The recordings were

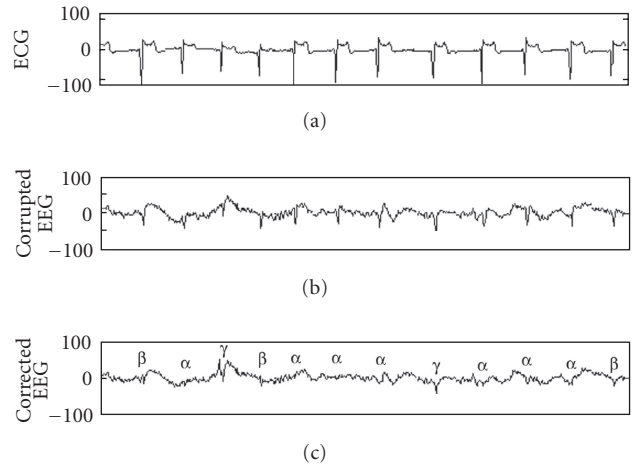

FIGURE 14: Examples of various peaks on the corrected signal-α: corrected peaks, β: half-corrected peaks, γ: uncorrected or very badly-corrected peaks.

taken from patients (7 males and 3 females aged between 40 and 73) with different pathologies (dysomnia, restless legs syndrome, insomnia, and apnoea/hypopnoea syndrome). They all contain cardiac interference as well as other typical artifacts (e.g., movement, sweat, respiration, etc.). The sampling rates were 50, 100, and 200 Hz. Only the ECG channel and the corrupted signal (EEG or EOG) were used to perform the ECG artifact correction. For each method, two hundred successive interference peaks of each excerpt were visually examined to compute the following:

(i) the number of corrected peaks (indicated as α on Figure 14);

(ii) the number of half-corrected peaks (indicated as β on Figure 14);

(iii) the number of uncorrected or very badly corrected peaks (indicated as γ on Figure 14).

A total of 2000 interference peaks were thus examined to compute the final correction rate.

Note that the distinction between "half-corrected peaks" and "very badly-corrected peaks" (although rather subjective) was only introduced to see whether a method, which cannot perfectly correct interference peaks, still brings some contribution. However, only perfectly-corrected peaks were considered to compute the correction rate.

On the basis of a first visual analysis of the results, some conclusions were already made.

First, we observed that the AF-ECG and ICA-ECG algorithms are unable to correct the cardiac artifact when the ECG is superimposed with slow waves due to breathing or sweating artifact. This led us to carry out a high-pass filtering of the ECG signal before the ECG artifact correction. The cutoff frequency of this filter was set to 1 Hz. The results obtained were conclusive, as illustrated in Figure 15 in the AF-ECG case.

We also found experimentally that the minimal order K of the filters in the AF and ICA methods has to be equal

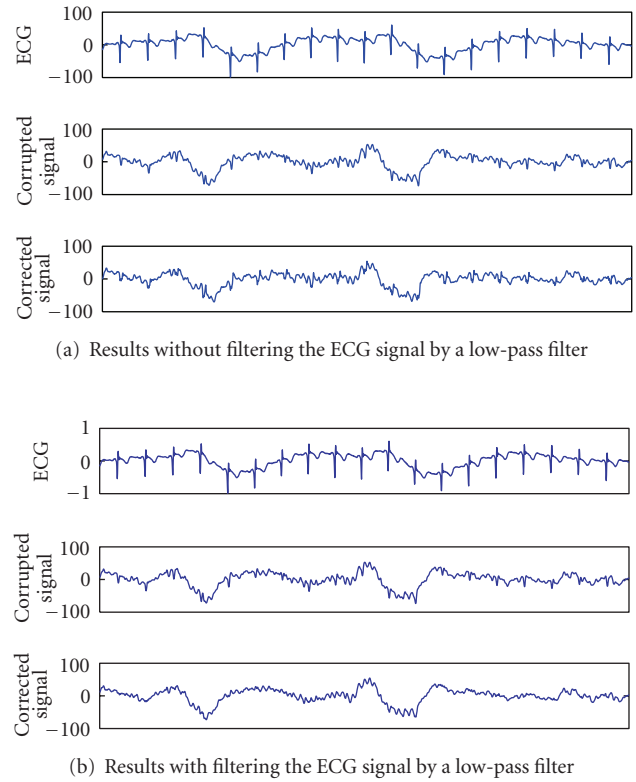

FIGURE 15: AF-ECG correction of the cardiac artifact in the presence of a slow wave on the ECG: (a) results without filtering the ECG by a low-pass filter, (b) result with filtering the ECG by a low-pass filter.

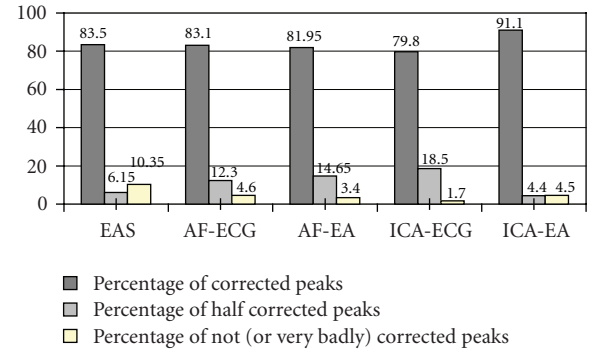

FIGURE 16: Global correction rates of the five processes computes on the 10 excerpts (2000 interference peaks).

to the average number of samples between the interference peaks and the ECG R-peak, plus four; a lower order leads to incomplete artifact correction and higher order increases the computational load without leading to better correction.

We, finally, noted that the results obtained with ICA were equivalent, whether the sigmoid function was logistic or hyperbolic; the convergence, however, was slower when using the logistic function.

As can be seen on the correction rates of the five processes (Figure 16), the first four algorithms exhibit quite similar correction rate, while our new method reaches a higher

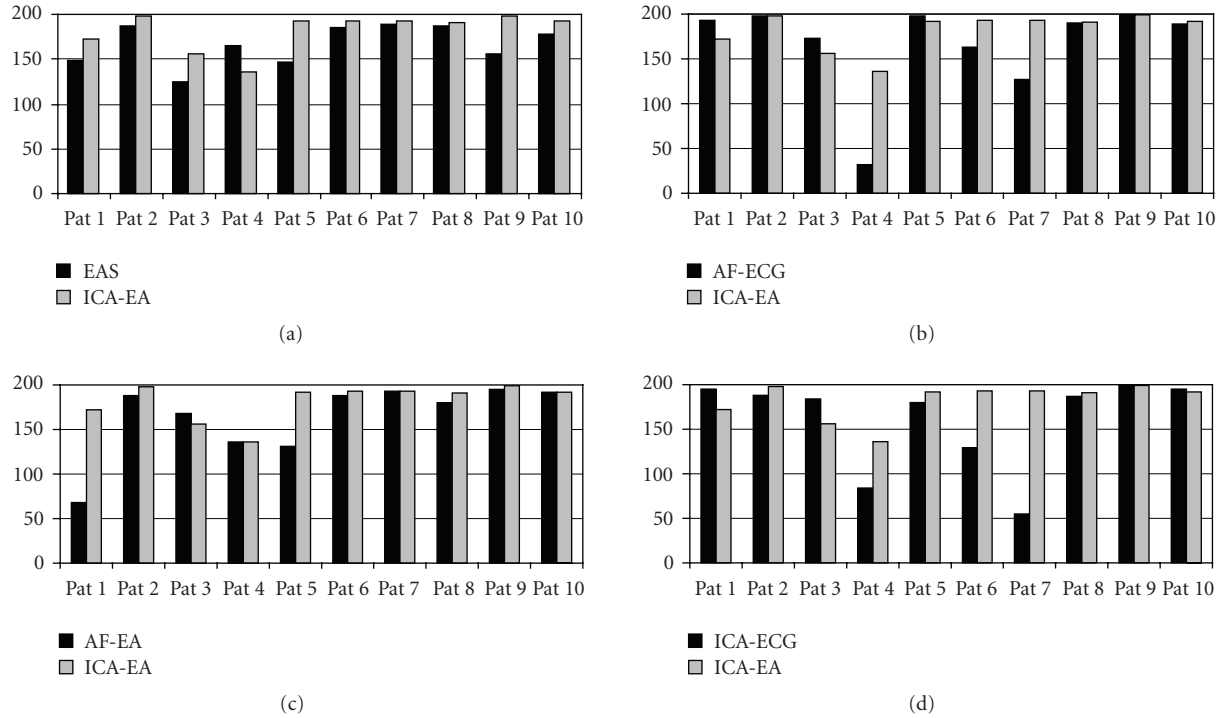

Figure 17: Comparison between the ICA-EA method and the four other algorithms: number of corrected peaks for each patient.

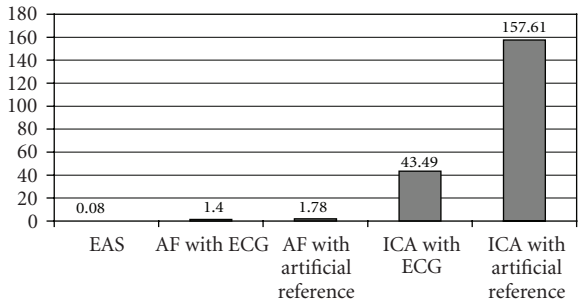

Figure 18: Average computing time (in seconds) to process a 15 minutes excerpt of polysomnographic signals in Matlab on a Pentium IV PC.

correction rate of 91.1% against 83.5% for ensemble average subtraction and 83.1% for adaptive filtering.

The highest percentage of uncorrected peaks is reached by the EAS algorithm. This is partly due to the difficulty of finding the exact position of the interference peaks on the EEG, especially when other artifacts are also present. Processes using an artificial reference are less affected by this problem since the ECG trigger (used to generate the artificial signal) is built on the ECG, which is less affected by artifacts, and in which the QRS complexes are more easily detectable.

Although using an artificial reference does not change much the percentage of corrected peaks in adaptive filtering, it does improve considerably the ICA results by considerably decreasing the number of half-corrected peaks while only slightly increasing the number of uncorrected peaks.

If we look at the number of corrected peaks obtained for each patient (Figure 17), we see that the ICA approach using an artificial reference is not systematically the algorithm which provides the best results. Its correction rate is sometimes higher than in the other methods and sometimes lower. However, while other methods sometimes completely fail on some excerpts (e.g., pat1 for AF-EA, pat4 for AF-ECG, and pat7 for ICA-ECG), the ICA-EA method always provides very satisfactory results. The reasons of this superiority will be discussed in Section 4, but we can already notice that the new method seems to be more robust to various types of polysomnographic signals than the other processes.

Unfortunately, ICA is significantly slower than EAS or AF (Figure 18 based on a Matlab implementation). This is due to the fact that it waits for the convergence of the underlying iterative process every 20-seconds fragment. What is more, convergence is slower when using an artificial observed signal, which increases the corresponding computational load.

Nevertheless, Matlab is clearly not optimized for the realization of iterative loops, which can partially explain the increases of computational load when using the ICA-based algorithms.

The ICA-EA method is thus very interesting for a posttreatment (such as that carried out before an automatic sleep stage classification), but is probably not suited for real-time use.

4. DISCUSSION

To carry out an automatic analysis of polysomnographic signals (such as a sleep stage classification) in a hospital, it is important for the system to be robust to the noise and independent of derivations used during the recording.

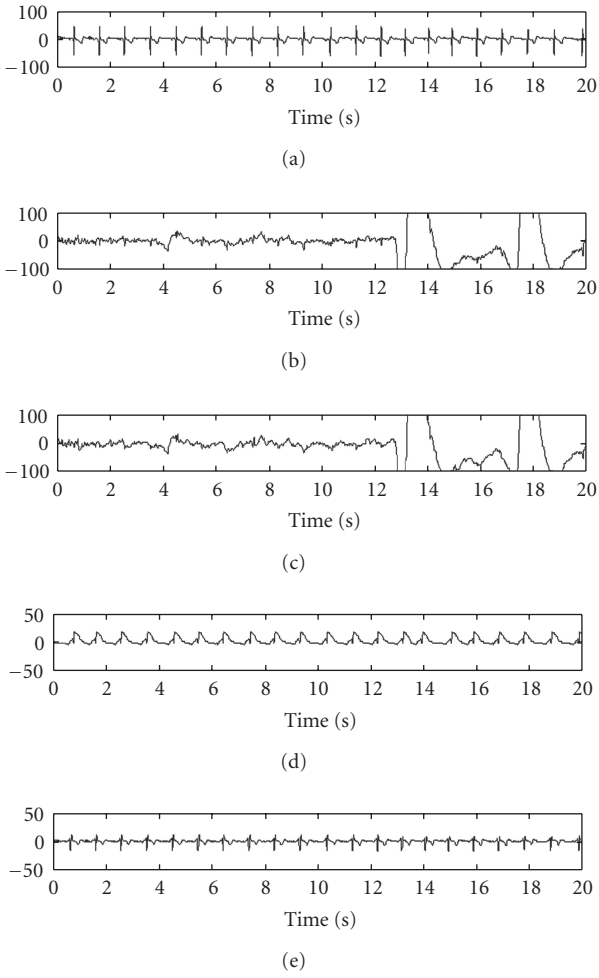

Figure 19: Results obtained on a 20 second excerpt from patient 10: (a) ECG, (b) corrupted signal, (c) correction by EAS, (d) estimate of the cardiac interference by the EAS methods, (e) estimate of the cardiac interference by ICA-EA.

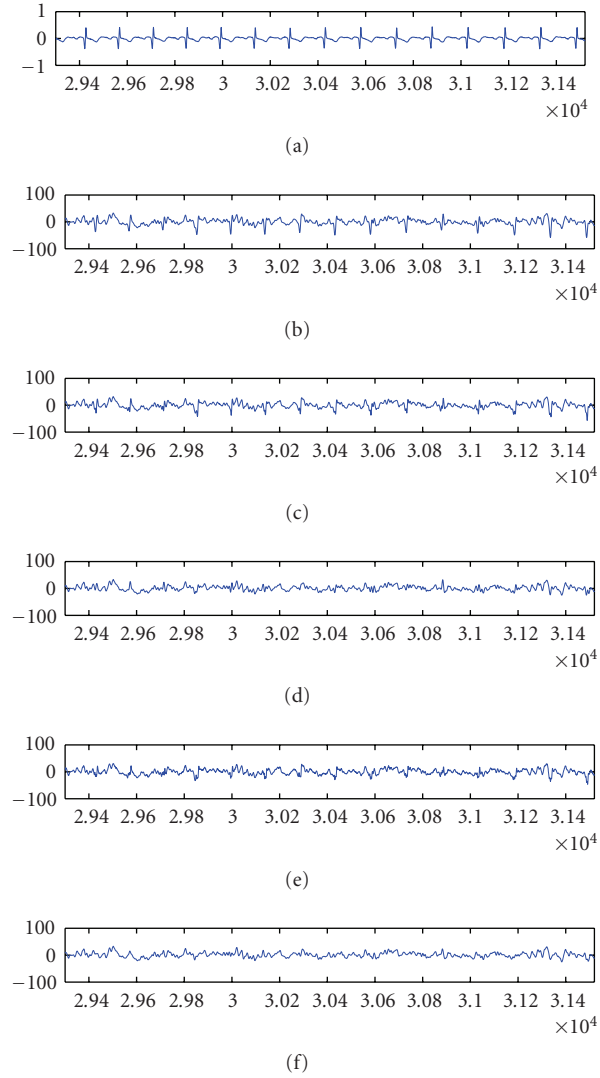

Figure 20: Results obtained on a 15 seconds excerpt from patient 4: (a) ECG, (b) corrupted signal, (c) correction by AF-ECG, (d) correction by AF-EA, (e) correction by ICA-ECG and (f) correction by ICA-EA.

The EAS algorithm is rather sensitive to noise. On one hand, the other artifacts (such as those due to eye blinks, movements, sweat, etc.) prevent an accurate detection of the interference peaks. On the other hand, these artifacts have a big influence on the computed average interference waveform. This is well illustrated on Figure 19. By looking at the cardiac interference estimate with the EAS method (Figure 19(d)), we can see that the position of the interference peak at the 14th second is not correctly detected because of artifact. Moreover, we see that the average interference waveform estimated by the EAS method seems to be strongly influenced by the artifact in contrast with the interference estimated by the ICA method (Figure 19(e)). This probably causes the bad corrections observed around seconds 4.5, 7.5, and 11 on Figure 19(c).

The AF-ECG and ICA-ECG methods are more robust to artifacts, but their performance completely fails for patients 4 and 7 (Figure 17). This is due to the fact that the cardiac interference waveform is rather different from the ECG signal in the polysomnographic recordings of these patients. The use of artificial reference is then very beneficial. As we can see on Figure 20, it facilitates convergence toward the correct solution, increasing the number of corrected peaks by the AF-EA and ICA-EA methods.

When the cardiac interference waveform is similar to that of the ECG, the artificial reference signal is also quite similar to the ECG (since it is obtained by averaging segments of corrupted signal located around each interference peak and by repeating this average artifact waveform each time the ECG trigger is different from zero). However, the slight differences between the artificial signal and the ECG can sometimes decrease the performance of the AF-EA and ICA-EA processes (patients 1 and 3 on Figure 17). Fortunately, this loss of performance is small compared with the increase in the number of corrected peaks when the cardiac interference waveform is different from that of the

ECG. In addition, it seems that adaptive filtering is more sensitive to this problem than the ICA method (Figure 17). This shows again the robustness of our new approach, this time to a slight modification of the reference.

Thus, we presented a new ECG artifact removal technique based on independent component analysis (ICA). The algorithm uses only two observed signals: the corrupted EEG (or EOG) and an artificial signal generated by repeating the average artifact waveform each time the ECG trigger is different from zero. An additional hypothesis is considered, which improve the convergence of the algorithm. The interference which is added to the EEG is assumed to be a filtered version of the artificial signal. Tests realized on simulated data showed that this new ICA algorithm has the minimum root mean squared error. Furthermore, using real data, we noted that this new method was much more robust to various waveforms of cardiac interference and to the presence of other artifacts than other tested processes (i.e., the ensemble average subtraction and the adaptive filtering). This probably explains why, on average, we found that our new algorithm was the most promising correction method with a correction rate of 91.1% against 83.5% for ensemble average subtraction and 83.1% for adaptive filtering. However, its high-computational load makes it hard to use in real-time systems.

ACKNOWLEDGMENTS

This work was partly supported by the Région Wallonne (Belgium) and the DYSCO Interuniversity Attraction Poles. Authors would like to thank Dr. François Meers for the impulse he gave to this project.

REFERENCES

[1] P. J. Allen, G. Polizzi, K. Krakow, D. R. Fish, and L. Lemieux, "Identification of EEG events in the MR scanner: the problem of pulse artifact and a method for its subtraction," *NeuroImage*, vol. 8, no. 3, pp. 229–239, 1998.

[2] C. Fortgens and M. P. De Bruin, "Removal of eye movement and ECG artifacts from the non-cephalic reference EEG," *Electroencephalography and Clinical Neurophysiology*, vol. 56, no. 1, pp. 90–96, 1983.

[3] J.-P. Lanquart, M. Dumont, and P. Linkowski, "QRS artifact elimination on full night sleep EEG," *Medical Engineering and Physics*, vol. 28, no. 2, pp. 156–165, 2006.

[4] M. Nakamura and H. Shibasaki, "Elimination of EKG artifacts from EEG records: a new method of non-cephalic referential EEG recording," *Electroencephalography and Clinical Neurophysiology*, vol. 66, no. 1, pp. 89–92, 1987.

[5] K. C. Harke, A. Schlögl, P. Anderer, and G. Pfurtscheller, "Cardiac field artifact in sleep EEG," in *Proceedings of the European Medical and Biological Engineering Conference (EMBEC '99)*, pp. 482–483, Vienna, Austria, November 1999.

[6] H.-J. Park, D.-U. Jeong, and K.-S. Park, "Automated detection and elimination of periodic ECG artifacts in EEG using the energy interval histogram method," *IEEE Transactions on Biomedical Engineering*, vol. 49, no. 12, part 2, pp. 1526–1533, 2002.

[7] Z. Sahul, J. Black, B. Widrow, and C. Guilleminault, "EKG artifact cancellation from sleep EEG using adaptive filtering," *Sleep Research*, vol. 24A, p. 486, 1995.

[8] P. Strobach, K. Abraham-Fuchs, and W. Harer, "Event-synchronous cancellation of the heart interference in biomedical signals," *IEEE Transactions on Biomedical Engineering*, vol. 41, no. 4, pp. 343–350, 1994.

[9] S. P. Cho, M. H. Song, Y. C. Park, H. S. Choi, and K. J. Lee, "Adaptive noise canceling of electrocardiogram artifacts in single channel electroencephalogram," in *Proceedings of the 29th Annual International Conference of IEEE Engineering in Medicine and Biology Society (EMBS '07)*, pp. 3278–3281, Lyon, France, August 2007.

[10] J. Iriarte, E. Urrestarazu, M. Valencia, et al., "Independent component analysis as a tool to eliminate artifacts in EEG: a quantitative study," *Journal of Clinical Neurophysiology*, vol. 20, no. 4, pp. 249–257, 2003.

[11] R. M. Everson and S. J. Roberts, "Independent component analysis," in *Artificial Neural Networks in Biomedicine*, P. J. G. Lisboa, E. C. Ifeachor, and P. S. Szczepaniak, Eds., pp. 153–168, Springer, Berlin, Germany, 2000.

[12] W. Zhou, "Removal of ECG artifacts from EEG using ICA," in *Proceedings of the 2nd Joint Engineering in Medicine and Biology, 24th Annual Conference and the Annual Fall Meeting of the Biomedical Engineering Society (BMES / EMBS '02)*, vol. 1, pp. 206–207, Houston, Tex, USA, October 2002.

[13] W. Zhou and J. Gotman, "Removal of EMG and ECG artifacts from EEG based on wavelet transform and ICA," in *Proceedings of the 26th Annual International Conference of the IEEE Engineering in Medicine and Biology Society (EMBS '04)*, vol. 1, pp. 392–395, San Francisco, Calif, USA, September 2004.

[14] R. Agarwal, J. Gotman, D. Flanagan, and B. Rosenblatt, "Automatic EEG analysis during long-term monitoring in the ICU," *Electroencephalography and Clinical Neurophysiology*, vol. 107, no. 1, pp. 44–58, 1998.

[15] S. Haykin, *Adaptive Filter Theory*, Prentice-Hall, Englewood Cliffs, NJ, USA, 1986.

[16] R. M. Rangayyan, *Biomedical Signal Analysis: A Case-Study Approach*, IEEE Press, New York, NY, USA, 2002.

[17] A. J. Bell and T. J. Sejnowski, "An information-maximization approach to blind separation and blind deconvolution," *Neural Computation*, vol. 7, no. 6, pp. 1129–1159, 1995.

[18] K. Torkkola, "Blind separation of convolved sources based on information maximization," in *Proceedings of IEEE Workshop on Neural Networks for Signal Processing*, pp. 423–432, Kyoto, Japan, September 1996.

[19] "MIT-BIH arrhythmia database—tape directory and format specification," Document BMEC TR00, Massachusetts Institute of Technology, Cambridge, Mass, USA, 1980, http://www.physionet.org/physiobank/database/mitdb.

Preliminary call for papers

The 2011 European Signal Processing Conference (EUSIPCO-2011) is the nineteenth in a series of conferences promoted by the European Association for Signal Processing (EURASIP, www.eurasip.org). This year edition will take place in Barcelona, capital city of Catalonia (Spain), and will be jointly organized by the Centre Tecnològic de Telecomunicacions de Catalunya (CTTC) and the Universitat Politècnica de Catalunya (UPC).

EUSIPCO-2011 will focus on key aspects of signal processing theory and applications as listed below. Acceptance of submissions will be based on quality, relevance and originality. Accepted papers will be published in the EUSIPCO proceedings and presented during the conference. Paper submissions, proposals for tutorials and proposals for special sessions are invited in, but not limited to, the following areas of interest.

Areas of Interest

- Audio and electro-acoustics.
- Design, implementation, and applications of signal processing systems.
- Multimedia signal processing and coding.
- Image and multidimensional signal processing.
- Signal detection and estimation.
- Sensor array and multi-channel signal processing.
- Sensor fusion in networked systems.
- Signal processing for communications.
- Medical imaging and image analysis.
- Non-stationary, non-linear and non-Gaussian signal processing.

Submissions

Procedures to submit a paper and proposals for special sessions and tutorials will be detailed at www.eusipco2011.org. Submitted papers must be camera-ready, no more than 5 pages long, and conforming to the standard specified on the EUSIPCO 2011 web site. First authors who are registered students can participate in the best student paper competition.

Important Deadlines:

Proposals for special sessions	15 Dec 2010
Proposals for tutorials	18 Feb 2011
Electronic submission of full papers	**21 Feb 2011**
Notification of acceptance	23 May 2011
Submission of camera-ready papers	6 Jun 2011

Webpage: www.eusipco2011.org

Organizing Committee

Honorary Chair
Miguel A. Lagunas (CTTC)

General Chair
Ana I. Pérez-Neira (UPC)

General Vice-Chair
Carles Antón-Haro (CTTC)

Technical Program Chair
Xavier Mestre (CTTC)

Technical Program Co-Chairs
Javier Hernando (UPC)
Montserrat Pardàs (UPC)

Plenary Talks
Ferran Marqués (UPC)
Yonina Eldar (Technion)

Special Sessions
Ignacio Santamaría (Unversidad de Cantabria)
Mats Bengtsson (KTH)

Finances
Montserrat Nájar (UPC)

Tutorials
Daniel P. Palomar (Hong Kong UST)
Beatrice Pesquet-Popescu (ENST)

Publicity
Stephan Pfletschinger (CTTC)
Mònica Navarro (CTTC)

Publications
Antonio Pascual (UPC)
Carles Fernández (CTTC)

Industrial Liaison & Exhibits
Angeliki Alexiou (University of Piraeus)
Albert Sitjà (CTTC)

International Liaison
Ju Liu (Shandong University-China)
Jinhong Yuan (UNSW-Australia)
Tamas Sziranyi (SZTAKI -Hungary)
Rich Stern (CMU-USA)
Ricardo L. de Queiroz (UNB-Brazil)